Astronomy & Astrophysics manuscript no. paper˙SMC˙I4 July 18, 2011
(DOI: will be inserted by hand later)

arXiv:1107.1592v1 [astro-ph.HE] 8 Jul 2011

Highly absorbed X-ray binaries in the *Small Magellanic Cloud*

G. Novara[1], N. La Palombara[1], S. Mereghetti[1], F. Haberl[2], M. Coe[3], M. Filipovic[4], A. Udalski[7], A. Paizis[1], W. Pietsch[2], R. Sturm[2], M. Gilfanov[5], A. Tiengo[1], J. Payne[4], D. Smits[6], A. De Horta[4]

[1] INAF-IASF, Istituto di Astrofisica Spaziale e Fisica Cosmica "G.Occhialini", Via Bassini 15, I–20133, Milano, Italy
[2] Max-Planck-Institut für extraterrestrische Physik, Giessenbachstraße, 85748 Garching, Germany
[3] School of Physics and Astronomy, University of Southampton, SO17 1BJ, UK
[4] University of Western Sydney, Locked Bag 1797, Penrith South DC, NSW 1797, Australia
[5] Max-Planck-Institut für Astrophysik, Karl-Schwarzschild-Straße 1, 85741 Garching, Germany
[6] Department of Mathematical Sciences, University of South Africa, UNISA, Pretoria 0003, South Africa
[7] Warsaw University Observatory, Aleje Ujazdowskie 4, 00-478 Warsaw, Poland

...

Abstract. Many of the high mass X-ray binaries (HMXRBs) discovered in recent years in our Galaxy are characterized by a high absorption, most likely intrinsic to the system, that can impede their detection at the softest X-ray energies. Exploiting the good coverage obtained with sensitive *XMM–Newton* observations, we have undertaken a search for highly absorbed X-ray sources in the Small Magellanic Cloud (SMC), which is known to contain a large number of HMXRBs. After a systematic analysis of 62 *XMM–Newton* SMC observations, we obtained a sample of 30 sources with evidence of an equivalent hydrogen column density larger than 3×10^{23} cm^{-2}. Five of these sources are clearly identified as HMXRBs, four being previously known (including three X-ray pulsars) and one, XMMU J005605.8–720012, being reported here for the first time. For the latter, we present optical spectroscopy confirming the association with a Be star in the SMC. The other sources in our sample have optical counterparts fainter than magnitude ∼16 in the V band, and many have possible NIR counterparts consistent with highly reddened early-type stars in the SMC. While their number is broadly consistent with the expected population of background highly absorbed active galactic nuclei, a few of them could be HMXRBs in which an early-type companion is severely reddened by local material.

Key words. galaxies: *Small Magellanic Cloud* – stars: emission–line, Be – X-rays: binaries

1. Introduction

Many observations of the Small Magellanic Cloud (*SMC*) in the X-ray energy band have led to the discovery of a large number of High Mass X-ray Binaries (HMXRBs). The number of known HMXRBs in the *SMC* (about one hundred, Liu et al. (2005)) is much larger than expected by scaling the number of these sources seen in the Milky Way according to the mass ratio of the two galaxies (M_{MW}/M_{SMC} ∼50). This has been interpreted as evidence of a recent episode of star formation in the *SMC* (Majid et al. (2004), Shtykovskiy & Gilfanov (2007), Antoniou et al. (2010)). It is remarkable that the *SMC* contains only one supergiant system, SMC X-1. All the other HMXRBs in the *SMC* consist of neutron stars accreting from Be type companions. Be X-ray binaries constitute also the largest class of HMXRBs in our Galaxy, but the relative number of supergiant systems is much higher than in the *SMC*, since 30 of the 114 Galactic HMXRBs (Liu et al. 2006) are confirmed or suspected supergiant systems.

Send offprint requests to: Giovanni Novara, novara@iasf-milano.inaf.it

Many new Galactic HMXRBs have been discovered in the past few years with the INTEGRAL satellite, thanks to high sensitivity in the hard X-ray range, coupled with an extensive monitoring of the Galactic plane. These observations led to the recognition of the new class of Supergiant Fast X-ray Transients (SFXT) and to the discovery of persistent supergiant systems characterized by a high absorption (equivalent column density above a few 10^{23} cm^{-2}), which escaped an earlier discovery because the high absorption severely suppresses their flux below 10 keV (see, e.g., Sidoli (2010), for a recent review).

To search for highly absorbed HMXRBs in the *SMC* we carried out a dedicated analysis of the *XMM–Newton* data collected during the large program for the *SMC* survey performed by Haberl & Pietsch (2008) and other observations of SMC targets. In Sect. 2, we describe the X-ray observations and data processing and in Sect. 3 we describe the source detection and selection criteria that led us to identify a sample of 30 highly absorbed sources. Five of them are confirmed HMXRBs, including four that were already known as X-ray binaries (Sect. 4). In Sect. 5 we present optical spectroscopy

of the new source, demonstrating that it is a Be system in the *SMC*. We finally discuss our results in Sect. 6.

2. X-ray observations and data processing

We analyzed the 62 *XMM–Newton* pointings of the *SMC* performed from 2001 May 31 to 2010 March 16 listed in Table 1. The three *EPIC* focal plane cameras (Turner et al. 2001; Strüder et al. 2001) were operated in standard *Full Frame* mode.

The data of each camera were processed independently using the standard *XMM–Newton Science Analysis Software* (*SAS*, v.10.0.0). We first used the tasks `emproc` and `epproc` to obtain the *MOS* and *pn* event files of each pointing. We then filtered out time intervals affected by high instrumental background induced by flares of soft protons (with energies below a few hundred keV). To avoid contributions from genuine X-ray source variability, this was done by examining light curves binned at 100 s for events with energies above 10 keV and PATTERN$\leq$4 or 0 for, respectively, the *MOS* peripheral CCDs and the whole *pn* camera; the good time intervals (GTI) were selected by adopting different count–rate thresholds for the different pointings and instruments. By selecting only events within GTI, we finally obtained three "clean" event lists for each observation (i.e. two for the *MOS* and one for the *pn* cameras), whose exposure times are reported in Table 1. The total net exposure times are respectively 1572 and 1598 ks for the *MOS* cameras, and 1361 ks for the *pn* one.

3. Source detection and selection criteria

We optimized our source detection strategy to select highly absorbed X-ray sources. To this aim, we simulated the expected *EPIC* count distributions for absorbed power–law spectra, with photon–index Γ in the range 1–2. We used two absorption components: the first one, with column density fixed at 6×10^{20} cm^{-2} and elemental abundances from Wilms et al. (2000), accounts for the foreground absorption in our Galaxy; for the second one, which accounts for the absorption in the SMC and is intrinsic to the source, we considered N_H values in the range 10^{22}–10^{24} cm^{-2}, and metal abundances of 0.2, as is typical of the SMC (Russell & Dopita 1992). We defined the *Hardness Ratio* HR = $(H-S)/(H+S)$), based on the count rates in the soft (S, 1–3 keV) and hard (H, 3–10 keV) energy ranges. These simulations showed that, for Γ = 2 and $N_H > 3 \times 10^{23}$ cm^{-2}, the fraction of the detected source counts with energies above 3 keV is at least 70 %, and that this fraction is even higher for lower values of Γ. In Fig. 1, we report the estimated HR values as a function of N_H, for both the *pn* and *MOS* cameras and different values of Γ. On the basis of these simulations, we adopted a HR threshold value of 0.7, in order to select sources with $N_H > 3 \times 10^{23}$ cm^{-2}.

For each observation in Table 1, we used the cleaned event file to produce merged images from the three cameras in the 1–3 and 3–10 keV energy ranges, according to the procedure described in detail in Baldi et al. (2002). For the 3–10 keV pn images, we excluded the energy range 7.8–8.2 keV, in order to reduce the instrumental background caused by the Cu line.

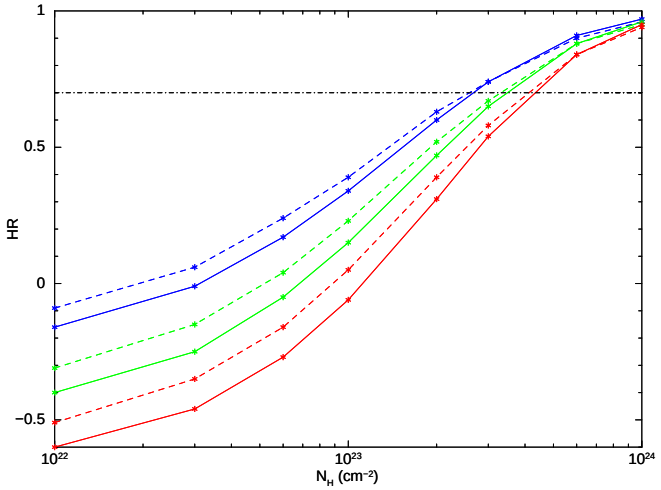

Fig. 1. Expected hardness ratio (of the count rates in the energy ranges 1–3 to 3–10 keV) as a function of the column density. Solid and dashed lines refer to the *pn* and the *MOS* cameras, respectively. Red, green, and blue lines refer to power-law spectra with photon indices of 2, 1.5, and 1, respectively. The horizontal line at HR = 0.7 represents the threshold value used to select highly absorbed sources.

For each image, we also produced the corresponding merged exposure map, which accounts for mirror vignetting and effective field of view. The total count-rate-to-flux conversion factors were obtained as a mean of the *MOS1/MOS2/pn* factors, weighted on the individual exposures of the three cameras. The source detection was based on a maximum likelihood technique, as described in detail in Novara et al. (2006), and used background maps produced with the correction algorithm described in Baldi et al. (2002). For each energy band, we only selected sources with a final detection likelihood -*ln P* $>$ 8.5 (where *P* is the probability of a false detection due to a Poissonian random fluctuation of the background). This likelihood threshold corresponds to a $\sim$3 σ detection. After manually removing a few spurious detections caused, for instance, by events falling close to the CCD edges, we obtained a final master list containing $\simeq$1500 sources. For each source, the master list provides various parameters including the detector and sky coordinates, the effective exposure time, the total counts, count–rate and errors in the different energy ranges, and the detection likelihood.

Table 1. Log of the *XMM–Newton* observations of 62 *SMC* fields with the corresponding net good time interval (GTI) for the two *MOS* and the *pn* cameras.

Observation ID	*XMM–Newton* revolution	Date (UT)	GTI (ks) MOS1	MOS2	pn
0011450101	0270	2001-05-31T02:20:10	42.8	43.0	40.8
0011450201	0355	2001-11-16T03:23:32	37.2	38.5	40.1
0018540101	0357	2001-11-20T23:42:37	26.7	27.0	23.4
0084200101	0422	2002-03-30T13:48:28	8.8	8.2	7.1
0084200801	0340	2001-10-17T10:07:40	20.7	20.7	17.1
0110000101	0156	2000-10-15T15:18:28	25.2	25.7	14.7
0110000301	0157	2000-10-17T21:45:54	12.6	12.4	7.4
0112780201	0143	2000-09-19T02:05:37	3.6	2.3	0.0
0112780601	0254	2001-04-29T21:07:59	0.9	1.5	2.9
0135721701	0721	2003-11-16T06:12:02	24.4	24.8	29.8
0142660801	0721	2003-11-17T03:55:54	7.2	7.5	6.8
0157960201	0737	2003-12-18T14:32:45	17.9	18.7	17.2
0164560401	0803	2004-04-28T22:08:04	0.2	0.1	0.1
0301170101	1151	2006-03-22T21:39:54	18.8	19.7	16.4
0301170201	1151	2006-03-23T04:48:17	22.5	22.7	14.4
0301170301	1158	2006-04-06T04:32:35	17.9	18.0	14.4
0301170601	1153	2006-03-27T12:21:01	14.4	14.5	11.7
0311590601	1146	2006-03-13T15:17:13	11.2	11.0	9.6
0402000101	1248	2006-10-03T00:09:09	21.7	21.7	19.0
0403970301	1329	2007-03-12T20:02:20	28.0	28.7	19.2
0404680201	1263	2006-11-01T00:56:29	32.4	32.4	30.8
0404680301	1344	2007-04-11T19:38:25	20.1	19.9	15.4
0404680501	1344	2007-04-12T03:07:23	23.3	23.7	21.6
0500980101	1380	2007-06-23T05:51:39	25.2	25.0	22.3
0500980201	1372	2007-06-06T08:52:16	27.6	28.3	14.1
0501470101	1371	2007-06-04T08:59:50	13.4	16.5	9.6
0503000201	1444	2007-10-28T05:49:58	21.5	21.5	20.0
0503000301	1514	2008-03-16T15:25:16	17.9	19.3	2.0
0601210101	1727	2009-05-14T09:14:24	20.7	21.2	19.8
0601210201	1794	2009-09-25T00:15:42	37.5	37.5	35.7
0601210301	1729	2009-05-18T10:29:15	30.9	31.4	27.5

Table 1. Continued

Observation ID	*XMM–Newton* revolution	Date (UT)	GTI (ks) MOS1	MOS2	pn
0601210401	1794	2009-09-25T11:22:24	37.6	37.6	36.0
0601210501	1794	2009-09-25T22:30:43	49.8	50.4	39.9
0601210601	1795	2009-09-27T00:10:53	36.7	37.1	32.7
0601210701	1795	2009-09-27T11:35:54	38.7	38.6	37.1
0601210801	1801	2009-10-09T18:33:30	24.7	24.7	23.1
0601210901	1795	2009-09-27T23:02:34	34.9	35.3	33.9
0601211001	1817	2009-11-09T21:16:08	34.0	35.0	23.7
0601211101	1806	2009-10-18T22:47:09	31.6	31.6	30.1
0601211201	1807	2009-10-20T22:51:09	33.1	33.2	29.0
0601211301	1798	2009-10-03T05:08:47	32.4	32.5	30.9
0601211401	1814	2009-11-04T21:38:31	35.3	35.6	31.1
0601211501	1803	2009-10-13T00:02:01	37.6	37.4	34.0
0601211601	1802	2009-10-11T22:43:47	31.6	32.3	28.8
0601211701	1804	2009-10-16T01:05:21	25.1	26.6	18.4
0601211801	1819	2009-11-13T20:59:56	26.2	30.2	22.3
0601211901	1827	2009-11-30T14:46:19	31.7	31.7	30.1
0601212001	1826	2009-11-27T22:39:06	28.3	28.3	26.3
0601212101	1820	2009-11-16T05:48:08	34.1	34.1	32.5
0601212201	1822	2009-11-16T06:10:27	27.1	29.4	24.3
0601212301	1786	2009-09-09T09:13:53	33.5	33.5	31.9
0601212401	1750	2009-06-29T14:46:19	29.5	30.9	23.9
0601212501	1786	2009-09-09T19:13:54	33.5	33.5	31.9
0601212601	1750	2009-06-29T06:04:39	26.0	27.1	17.5
0601212701	1840	2009-12-26T07:25:22	36.7	36.7	34.5
0601212801	1831	2009-12-07T23:35:54	21.3	21.3	16.7
0601212901	1788	2009-09-13T13:29:26	36.1	36.1	34.5
0601213001	1788	2009-09-13T01:11:03	41.6	41.7	38.9
0601213201	1878	2010-03-12T00:56:15	12.5	13.2	9.4
0601213301	1878	2010-03-12T05:26:15	9.8	9.9	8.1
0601213401	1880	2010-03-16T10:05:12	17.6	17.5	11.9
0656780201	1886	2010-03-27T12:20:41	11.0	12.3	7.0

Table 2. Main characteristics of the highly absorbed X-ray sources.

(1) SRC	(2) NAME	(3) RA h:m:s	(4) DEC ○:′:″	(5) ERROR arcsec	(6) Likelihood	(7) RATE ($\times 10^{-4}$ cts s^{-1})	(8) f_X erg cm^{-2} s^{-1}	(9) HR	(10) Remarks
01	XMMUJ004102.6–732530	00:41:02.69	–73:25:30.9	2.1	27.43	13.6 ± 2.9	8.94E–14	0.86 ± 0.23	
02	XMMUJ004210.9–733011	00:42:10.90	–73:30:11.8	2.0	16.80	12.4 ± 3.3	8.21E–14	1.00 ± 0.29	
03	XMMUJ004226.3–730417	00:42:26.38	–73:04:17.4	1.5	37.07	11.7 ± 2.0	7.76E–14	0.73 ± 0.20	
04	XMMUJ004244.7–732356	00:42:44.77	–73:23:56.4	2.1	15.34	5.9 ± 1.6	3.89E–14	0.80 ± 0.34	
05	XMMUJ004536.2–724131	00:45:36.23	–72:41:31.3	1.7	10.74	18.4 ± 5.8	1.18E–13	0.73 ± 0.29	
06	XMMUJ004814.0–731006	00:48:14.07	–73:10:06.0	1.5	58.28	55.4 ± 8.2	3.49E–13	0.73 ± 0.12	XMMUJ004814.1-731003, SXP25.5 (1)
07	XMMUJ004818.7–732102	00:48:18.74	–73:21:02.4	1.9	>86	103 ± 9.1	6.81E–13	0.81 ± 0.08	[SG2005] SMC 34 (2)
08	XMMUJ004853.5–732455	00:48:53.51	–73:24:55.7	2.0	>86	84.3 ± 8.2	5.71E–13	0.72 ± 0.07	
09	XMMUJ004911.5–731717	00:49:11.57	–73:17:17.8	1.8	12.79	15.1 ± 4.8	9.86E–14	0.91 ± 0.34	CXOU J004910.7-731717 (3)
10	XMMUJ005020.7–720907	00:50:20.74	–72:09:07.0	0.6	>86	68.6 ± 5.3	4.51E–13	0.94 ± 0.05	
11	XMMUJ005306.6–722400	00:53:06.66	–72:24:00.2	1.5	12.96	6.0 ± 1.8	3.93E–14	0.72 ± 0.33	
12	XMMUJ005322.4–715927	00:53:22.44	–71:59:27.5	1.0	10.35	11.2 ± 3.6	7.41E–14	0.87 ± 0.36	
13	XMMUJ005605.8–720012	00:56:05.85	–72:00:12.2	1.6	26.57	8.4 ± 1.7	5.51E–14	0.70 ± 0.23	New Be binary
14	XMMUJ005722.4–713114	00:57:22.44	–71:31:14.8	0.9	12.66	15.7 ± 4.3	1.03E–13	0.72 ± 0.33	
15	XMMUJ005724.3–715917	00:57:24.31	–71:59:17.8	1.5	16.81	17.8 ± 4.6	1.20E–13	0.84 ± 0.29	
16	XMMUJ005732.5–712926	00:57:32.51	–71:29:26.3	1.8	8.93	11.3 ± 3.7	7.48E–14	0.86 ± 0.46	
17	XMMUJ005735.8–721935	00:57:35.82	–72:19:35.1	2.0	30.99	21.4 ± 4.5	1.45E–13	1.00 ± 0.18	XMMU J005735.7-721932 (4) CXOU J005736.2-721934, SXP565 (5)
18	XMMUJ005812.9–723049	00:58:12.92	–72:30:49.5	1.4	>86	1330 ± 30	8.78E–12	0.77 ± 0.01	RX J0058.2-7231, SXP293 (6)
19	XMMUJ010115.2–721640	01:01:15.28	–72:16:40.6	2.1	13.14	19.7 ± 5.5	1.30E–13	0.82 ± 0.35	
20	XMMUJ010233.9–723443	01:02:33.99	–72:34:43.2	1.8	60.86	29.7 ± 4.9	1.90E–13	0.91 ± 0.17	
21	XMMUJ010248.6–730822	01:02:48.69	–73:08:22.6	1.4	39.22	28.2 ± 6.2	1.83E–13	0.77 ± 0.23	
21	XMMUJ010432.5–722543	01:04:32.56	–72:25:43.6	2.1	12.73	8.9 ± 2.5	5.81E–14	0.85 ± 0.36	
23	XMMUJ010802.9–722627	01:08:02.93	–72:26:27.5	2.1	17.50	7.9 ± 2.2	5.21E–14	0.71 ± 0.30	
24	XMMUJ010811.9–721005	01:08:11.91	–72:10:05.2	1.2	24.42	7.0 ± 1.6	4.61E–14	0.81 ± 0.27	
25	XMMUJ010831.4–730630	01:08:31.40	–73:06:30.9	1.6	39.61	12.1 ± 2.1	7.98E–14	0.93 ± 0.19	
26	XMMUJ010842.6–723839	01:08:42.68	–72:38:39.6	1.8	25.94	39.5 ± 8.0	2.56E–13	0.79 ± 0.17	
27	XMMUJ010908.0–720642	01:09:08.09	–72:06:42.1	1.3	13.52	6.3 ± 1.9	4.11E–14	0.85 ± 0.35	
28	XMMUJ011339.7–724733	01:13:39.74	–72:47:33.3	2.0	11.87	15.0 ± 4.8	1.01E–13	0.86 ± 0.31	
29	XMMUJ011434.8–730730	01:14:34.83	–73:07:30.4	2.2	10.66	14.7 ± 4.7	9.70E–14	0.70 ± 0.29	
30	XMMUJ011807.8–731713	01:18:07.84	–73:17:13.9	2.2	16.17	24.6 ± 6.3	1.60E–13	0.85 ± 0.23	

Key to Table: Col.(1) = source ID; Col.(2) = source catalogue name; Col.(3) = right ascension (J2000); Col.(4) = declination (J2000); Col.(5) = position error (1 σ c.l.); Col.(6) = detection likelihood; Col.(7) = 3–10 keV count rate (sum of the PN and MOS counts divided by the sum of PN and MOS exposures); Col.(8) = X-ray flux in the energy band 3–10 keV, assuming a power–law emission model with a hydrogen column density $N_H > 3 \times 10^{23}$ cm^{-2} and a photon–index Γ = 1.5; Col.(9) = hardness ratio between energy bands 1–3 keV and 3–10 keV; Col.(10) = likely identification with already known sources. References are given in parenthesis:

(1) Haberl et al. (2008b) (2) Shtykovskiy & Gilfanov (2005) (3) Laycock et al. (2010) (4) Sasaki et al. (2003), Haberl et al. (2008a) (5) Macomb et al. (2003) (6) Haberl et al. (2008a) (7) McGowan et al. (2008)

4. Results

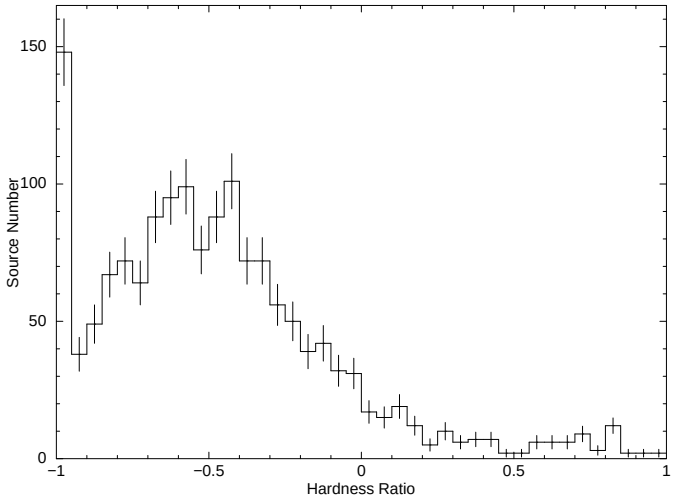

Fig. 2. Hardness-ratio distribution of the detected X–ray sources

In Fig. 2, we report the HR distribution of all the detected sources. This figure illustrates that most sources have HR < 0, with a peak around -0.5, hence they are characterized by non-absorbed soft spectra. On the other hand, only very few sources have high HR values. In our final source list, there are 30 objects with HR > 0.7, which we consider as highly absorbed sources with $N_H > 3 \times 10^{23}$ cm^{-2}; given the HR distribution, we expect that, even if we take into account the HR errors, only a very few additional sources would have HR > 0.7. The sky coordinates of these 30 objects, corrected for the satellite pointing uncertainty, are listed in Table 2. The astrometric correction of the X-ray images was done by cross–matching the brightest sources of each field with the Magellanic Clouds Photometric Survey optical catalogue (MCPS, Zaritsky et al. (2002)), and selecting the X-ray sources with a single, clearly evident optical counterpart within a 3″ error radius. We then used the IRAF task `geomap` to compute the linear transformation between the X-ray and optical coordinates of these reference sources. The calculated X-ray–to–optical coordinate transformations have rms fit residuals between 0.″43 and 1.″85 at 1 σ c.l., with an average value of 1.″1; they correspond to the (radial) systematic astrometric errors in the corrected observations. These transformations were then used by the IRAF task `geoxytran` to obtain the corrected X-ray coordinates given in Table 2. The total uncertainty on the X-ray position of each source is given by the sum in quadrature of the calculated systematic astrometric error in the observation and the measured statistical error of the source itself.

We also list in Table 2 the hardness ratios, count rates, and fluxes of the sources. The fluxes refer to the 3–10 keV energy range, and have been computed assuming a power-law with photon index Γ = 1.5 and $N_H = 3\times10^{23}$ cm^{-2}. The brightest source has a absorbed flux of 9×10^{-12} erg cm^{-2} s^{-1}, while the faintest sources in our sample have fluxes of $\sim4\times10^{-14}$ erg cm^{-2} s^{-1} corresponding to $\sim2\times10^{34}$ erg s^{-1}, assuming a *SMC* distance of 60 kpc (Hilditch et al. 2005)

Some of our selected sources were already reported in other studies of the *SMC*, in these cases we give in the table their original name and the relevant references. Four sources, including three pulsars, were already known as HMXRBs: SXP25.5, SMC34, SXP565, and SXP293. We searched for possible counterparts of our highly absorbed sources using the MCPS catalogue, which is based on observations performed in the *U*, *B*, *V*, and *I* filters between November 1996 and December 1999 (Zaritsky et al. 2002), and the InfraRed Survey Facility (IRSF) Magellanic Cloud catalogue (Kato et al. 2007) for the NIR (*J*, *H* , and *K* filters).

For each source, we report in Table 3 the optical and NIR properties of the brightest object in the K band present within a distance equal to two times the 1 σ position error (with only five exceptions, marked in the table, the brightest object in K is also the brightest in V). For five sources, no catalogued optical or NIR counterparts were found to limits as faint as of V$\sim$23 mag and K$\sim$17 mag.

A plot of the NIR versus optical colors shows that the four already known HMXRBs of our sample are located in the region corresponding to J–K$<$0.5 mag and B–V$<$0.5 mag (see Fig. 3). As discussed in Sect. 5, the other source falling in this region (source # 13) is a new Be binary system in the SMC. Three of these sources are well above the position of the main–sequence stars (whose colors are taken from Johnson (1966)): if they are affected by an IR excess (which could be due to the decretion disk of the Be star), their optical/NIR colors are consistent with early-type stars with moderate optical reddenings ($A_V \sim$ 2–3 mag). On the other hand, HMXRBs in which the optical companion is also affected by a high local absorption would show much redder colors, as seen in several of the new HMXRBs discovered by INTEGRAL in our Galaxy. Therefore, we cannot exclude that some of the other sources plotted in Fig. 3, or sources for which no optical and NIR counterparts have been detected, are also highly absorbed HMXRBs. The five sources at the top of the plot are far from the main–sequence stars, therefore it is difficult to suggest a reliable classification of them; this is particularly true for the three sources shown as open circles, for which a different counterpart could also be suggested. These five sources could be early-type stars only if they are characterized by both a large IR excess and a high reddening. On the other hand, since for AGNs J–K > 0.5 (Kouzuma & Yamaoka 2010) and -0.4 $<$ B–V < 0.7 (Hatziminaoglou et al. 2002), these sources could be more probably classified as reddened AGNs.

To search for possible periodicities in any optical counterparts close to the *XMM–Newton* sources, data from OGLE III were acquired for all objects within 4″ of the 30 *XMM–Newton* position. We applied a Lomb-Scargle analysis to a total of 129 lightcurves, searching for periods in the range 2–200 days. Periods shorter than 2 days were avoided because they are getting close to the average daily sampling of the OGLE data, and periods longer than 200 days approach the annual sampling patterns. In each case, the data were first de-trended using a polynomial of order three before being searched. In some cases, there were many optical counterparts; conversely, other sources had no optical objects within the search zone.

Table 3. Candidate optical-IR counterparts of the highly absorbed X-ray sources.

(1) ID	(2) NAME	(3) V mag	(4) f_X/f_V $\log_{10}$	(5) K mag	(6) B–V mag	(7) J–K mag
01	IRSF 00410291-7325332	20.79$^{(a)}$	0.76	16.68	1.21	1.61
02	IRSF 00421082-7330127	19.31$^{(a)}$	0.13	17.00	1.05	0.63
03	IRSF 00422638-7304184	>23	>1.58	15.65	-	2.02
04	IRSF 00424550-7323553	17.05	-1.09	13.90	1.39	0.87
05	IRSF 00453646-7241343	19.43	0.34	15.72	0.73	1.84
06	IRSF 00481410-7310040	15.30	-0.85	15.64	0.26	0.04
07	IRSF 00481871-7321000	16.18	-0.21	15.29	0.25	0.36
08	IRSF 00485330-7324574	>23$^{(a)}$	>2.44	15.55	-	1.30
09	IRSF 00491089-7317172	18.80	0.01	15.95	1.00	0.38
10	IRSF 00502062-7209073	>23	2.34	16.86	-	1.65
11	?	>23	>1.28	>17	-	-
12	MCPS 2493874	20.74	0.65	>17	0.47	-
13	IRSF 00560575-7200118	16.71	-1.08	17.18	-0.11	-0.11
14	?	>23	>1.70	>17	-	-
15	MCPS 3076421	21.42	1.14	>17	0.35	-
16	?	>23	>1.56	>17	-	-
17	IRSF 00573600-7219342	15.99	-0.95	15.35	0.01	0.42
18	IRSF 00581258-7230488	14.87	0.38	14.14	0.10	0.39
19	IRSF 01011529-7216374	19.23$^{(a)}$	0.30	14.69	1.28	1.59
20	IRSF 01023342-7234421	19.64$^{(a)}$	0.62	16.09	1.14	1.68
21	IRSF 01024839-7308213	20.99	1.15	17.08	1.04	1.90
22	IRSF 01043305-7225407	16.23	-1.25	13.12	1.38	0.81
23	MCPS 4411974	20.01	0.21	>17	0.04	-
24	IRSF 01081153-7210048	>23	>1.35	17.26	-	1.61
25	IRSF 01083147-7306325	18.00	-0.41	15.84	0.98	0.50
26	IRSF 01084310-7238375	19.53	0.71	17.84	0.84	0.21
27	IRSF 01090778-7206438	21.13	0.55	>17	0.57	-
28	MCPS 4879163	22.36	1.44	>17	0.56	-
29	?	>23	>1.67	>17	-	-
30	?	>23	>1.89	>17	-	-

Key to Table: Col.(1) = source ID; Col.(2) = name of the brightest infrared (IRFS sources, (Kato et al. 2007)) or optical (MCPS sources, (Zaritsky et al. 2002)) candidate counterpart within the X–ray error circle (a '?' is reported when no counterpart is found); Col.(3) = *V* magnitude; Col.(4) = X-ray–to–optical flux ratio (in $\log_{10}$ units); Col.(5) = *K* magnitude; Col.(6) = *B–V* color index; Col.(7) = *J–K* color index
Notes $^{(a)}$ for this object there is a possible counterpart with a slightly brighter V magnitude.

Significant periodicities were found for four sources (three of which were already known) and tentative periods for an additional three objects (see Table 4). That three previously known periods were "re-discovered" in this search reassures us that the techniques used are effective in identifying possible periods. The one new significant detection (source number 19) shows a modulation that is extremely sinusoidal in nature when the data are folded at the period of 199.6 days. This modulation shape is not normal for a long-period binary modulation, which tends to reveal short outbursts coincident with the periastron passage of the neutron star (see, for example, Coe & Edge (2004)). Such smooth sinusoidal modulations tend to be associated with pulsations in stars. A likely possibility is that it could be an Non-Radial Pulsations (NRP) in a B-type star with a period very close to the one day sampling, with the result that the signal at 199.6 days is the beat frequency of the true pulse period and the sampling period.

5. XMMU J005605.8–720012: A new Be HMXRB in the *SMC*

Source # 13 was detected with a total of 68 counts in the hard energy range 3–10 keV and a HR value of 0.71, just above our threshold. It has a relatively bright (V = 16.71 mag) optical counterpart, with color B–V = –0.12 mag, and with a quality flag in the MCPS indicating a successful fit with a stellar atmosphere model. It has an unabsorbed luminosity, in the energy range 3–10 keV, of 4.4×10^{34} erg s^{-1}.

Optical spectral observations of source # 13 were obtained in September 2010, using the 1.9-meter telescope and the Cassegrain spectrograph at the South African Astronomical Observatory (SAAO) in Sutherland. We used grating number 7 (300 lines per mm) to obtain spectra between 3700 Å and 7700 Å at a resolution of 5 Å. For these, the slit size was $1\farcs5 \times 1\farcm5$. Exposure times were limited to 900 s with a positional accuracy of $< 1''$. Data reduction included bias subtraction and flat-field correction using the IRAF software package. Extraction (task

Table 4. List of OGLE III objects within 4" of an *XMM–Newton* position that show evidence of a periodic signal

XMM ID	OGLE III ID	V	I	LS power	Period	Comments
2	22605	21.3	20.3	12	2.16 days	Tentative
6	50768	15.8	15.7	14	22.5 days	SXP25.5 (Rajoelimanana et al. 2011)
8	20669	?	21.0	13	4.08 days	Tentative
17	27992	16.1	15.8	26	157.2 days	SXP565 (Bird et al. 2011)
18	19191	14.9	14.6	200	59.7 days	SXP293 (Schmidtke et al. 2004)
20	43690	20.8	21.0	15	5.96 days	Tentative
26	22676	19.6	18.6	23	199.6 days	Possible new period

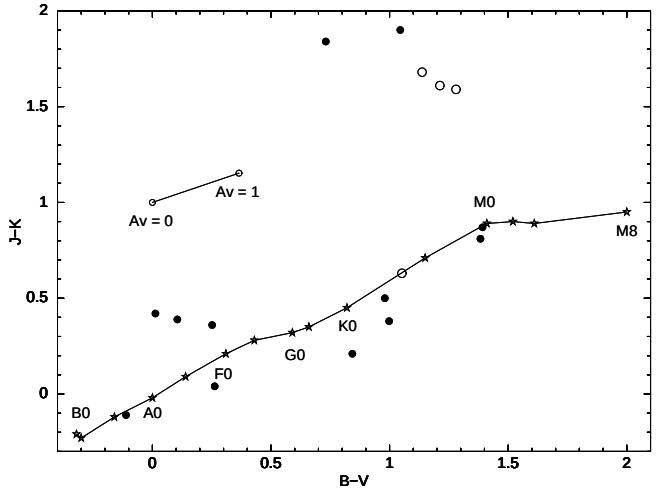

Fig. 3. Color indicies of the candidate counterparts of the highly absorbed X-ray sources of our sample. For the sources reported with a filled circle, the brightest optical and infrared candidate counterparts are coincident, while the sources reported as an open circle correspond to those with the 'a' flag in Table 3: in this case, there is also a possible alternative counterpart, with a slightly brighter V magnitude, to the selected infrared counterpart. We also indicate the main-sequence stars and a bar which shows the reddening corresponding to A_V=1 mag.

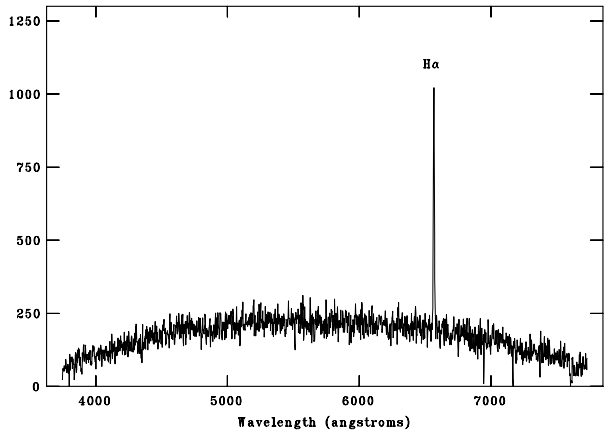

Fig. 4. SAAO optical spectrum of source # 13; note the presence of a strong H_α emission line.

`extractor`), including background sky subtraction, of data allowed the creation of one–dimensional spectra, wavelength calibrated using standard lines from a Cu-Ar arc. Observing conditions were not photometric, seeing was limited to 2″ at best but varied throughout the evening. We show in Fig. 4 the resulting spectrum: its moderate signal–to–noise ratio does not allow us to make a spectral classification, but a significant H_α emission line, with equivalent width EW = –37.44 Å, is clearly visible.

Despite no periodicities being found in the OGLE light curve of this star, these findings indicate that source # 13 is a Be HMXRB. Since sources of this class typically have a transient nature, we searched for hard X-ray outbursts in all the public data obtained with the *INTEGRAL* satellite (Winkler et al. 2003), that is all pointings obtained with the IBIS instrument (Ubertini et al. 2003) in which the source position was within 12 degrees from the center of the field of view. This led to a total of 619 pointings, with different exposure times from about 1800 sec to about 3600 sec, spanning from July 2003 to June 2009. We used version 9.0 of the Off-line Scientific Analysis software to analyse the data. For each pointing we extracted an image in the 17–40 keV energy band, but in none of them was the source significantly detected. The typical flux upper limit of the individual images is on the order of ∼20 mCrab. We also produced a deep image by summing all the individual pointings, reaching a total exposure of about 2 Msec. The source was not detected, with a 5 σ upper limit of about 1 mCrab in the 17–40 keV range, which is well above the extrapolation of the flux seen by *EPIC*.

6. Discussion

We have detected 30 sources with hardness ratios indicating a column density $N_H > 3 \times 10^{23}$ cm^{-2}. Five of these sources are HMXRBs, of which one was discovered in our search and spectroscopically identified as a new Be binary system. Most of the remaining 25 sources have very faint (V>18) or no optical counterparts, with colors not compatible with reddened early type-stars (unless a significant IR excess is present). Therefore, they can hardly be considered as candidate absorbed HMXRBs.

Spectral information for a few of the brightest sources of our sample was previously reported in other works. The *XMM–Newton* spectrum of the 25 s pulsar XMMU J004814.1–731003 was closely fit with a power law of photon index 1.33±0.27 and $N_H = 5 \times 10^{22}$ cm^{-2}, confirming our conclusion that it

is a highly absorbed source. Our brightest source (# 18) is the 293 s pulsar RX J0058.2–7231, for which Haberl et al. (2008a) reported an absorption $N_H = (1.35 \pm 0.32) \times 10^{22}$ cm^{-2}, considerably smaller than the value we inferred from the hardness ratio. This might be due to the results of Haberl et al. (2008a) being obtained from the June 2007 *XMM–Newton* observation, while our results for this source are based on the SMC Survey pointing carried out in October 2009, when the source was about a factor of ten brighter. HMXRBs can display large variations in their intrinsic absorption, as shown for example in the case of the long period (1323 s) SMC pulsar RXJ0103.6–7201 (Eger & Haberl 2008).

We do not expect of course all the sources in our sample to be HMXRBs in the SMC. A large fraction of them will turn out to be background-absorbed AGNs. On the other, hand our sample should not contain foreground stars belonging to our Galaxy, which would show softer and less absorbed X-ray spectra.

A rough estimate of the number of absorbed AGNs in our sample can be derived using published number flux relations for extragalactic sources. For example, based on the LogN-LogS relations for AGNs with $N_H = 3 \times 10^{23}$ cm^{-2} by Gilli et al. (2007), we obtain a surface density of $\sim$4 AGNs per square degree at a flux limit of 4×10^{-14} erg cm^{-2} s^{-1}. Our survey covered a sky area of $\sim$5 square degrees, although with a non-uniform sensitivity, because of telescope vignetting and different exposure times. Owing to the uncertainties in the LogN-LogS relations and the small number of objects, this prediction is consistent with the number of unidentified sources in our sample.

7. Conclusions

Motivated by the presence of several highly absorbed HMXRBs in our Galaxy, we have carried out a search for similar systems in the *SMC* exploiting the nearly complete coverage of this galaxy obtained with *XMM–Newton*. Our selection criteria, corresponding to an absorption threshold of $\sim 3 \times 10^{23}$ cm^{-2}, were met by four known HMXRBs and led to the discovery of a new highly absorbed Be binary in the SMC. We also selected other 25 additional sources, among which other highly absorbed HMXRBs might be present. Since we also expect a good fraction of these sources to be AGNs, we can say that the SMC does not contain much more than $\sim$10 persistent HMXRBs with intrinsic $N_H > 3 \times 10^{23}$ cm^{-2}. We cannot exclude the presence of a much larger population of intrinsically absorbed binaries of transient nature, which could not be detected in our survey if their quiescent luminosity is below a few 10^{34} erg s^{-1}.

Acknowledgments

Acknowledgements. We wish to thank Lara Sidoli for the useful discussion. This work is based on observations obtained with *XMM–Newton*, an ESA science mission with instruments and contributions directly funded by ESA Member States and NASA. The *XMM–Newton* data analysis is supported by the Italian Space Agency (ASI) (ASI/INAF contract I/032/10/0). We were granted observation time at the South African Astronomical Observatory (SAAO) and wish to thank them for their kind help and accommodations. Travel to the SAAO was funded by Australian Government AINSTO AMNRF grant number 10/11-O-06. Partly based on observations with *INTEGRAL*, an ESA project with instruments and science data centre funded by ESA member states (especially the PI countries: Denmark, France, Germany, Italy, Spain, and Switzerland), Czech Republic and Poland, and with the participation of Russia and the USA. IRAF is the Image Reduction and Analysis Facility, a general purpose software system for the reduction and analysis of astronomical data. IRAF is written and supported by the IRAF programming group at the National Optical Astronomy Observatories (NOAO) in Tucson, Arizona. NOAO is operated by the Association of Universities for Research in Astronomy (AURA), Inc. under cooperative agreement with the National Science Foundation. Extractor is part of an IRAF package (PNDR) developed to assist with the efficient reduction of long-slit spectra of emission line objects. It was developed as part of the Macquarie/AAO/Strasbourg Halpha (MASH) Planetary Nebulae Catalogue.

References

Antoniou, V., Zezas, A., Hatzidimitriou, D., & McDowell, J. C. 2009, ApJ, 697, 1695
Antoniou, V., Zezas, A., Hatzidimitriou, D., & Kalogera, V. 2010, ApJ, 716, L140
Baldi, A., Molendi, S., Comastri, A., et al. 2002, ApJ, 564, 190
Bird, A. J., Coe, M. J., & McBride, V. 2011, MNRAS, (submitted)
Coe, M. J., & Edge, W. R. T. 2004, MNRAS, 350, 756
Eger, P., & Haberl, F. 2008, A&A, 491, 841
Galache, J. L., Corbet, R. H. D., Coe, M. J., Laycock, S., Schurch, M. P. E., Markwardt, C., Marshall, F. E., & Lochner, J. 2008, ApJS, 177, 189
Gilli, R., Comastri, A., & Hasinger, G. 2007, A&A, 463, 79
Haberl, F., Eger, P., & Pietsch, W. 2008a, A&A, 489, 327
Haberl, F., Eger, P., Pietsch, W., Corbet, R. H. D., & Sasaki, M. 2008b, A&A, 485, 177
Haberl, F., & Pietsch, W. 2008, X-rays From Nearby Galaxies, 32
Hatziminaoglou, E., et al. 2002, A&A, 384, 81
Hilditch, R. W., Harries, T. J., & Howarth, I. D. 2005, Highlights of Astronomy, 13, 455
Johnson, H. L. 1966, ARA&A, 4, 193
Kato, D., et al. 2007, PASJ, 59, 615
Kouzuma, S., & Yamaoka, H. 2010, A&A, 509, A64
Laycock, S., Zezas, A., Hong, J., Drake, J. J., & Antoniou, V. 2010, ApJ, 716, 1217
Liu, Q. Z., van Paradijs, J., & van den Heuvel, E. P. J. 2005, A&A, 442, 1135
Liu, Q. Z., van Paradijs, J., & van den Heuvel, E. P. J. 2006, VizieR Online Data Catalog, 345, 51165
Macomb, D. J., Fox, D. W., Lamb, R. C., & Prince, T. A. 2003, ApJ, 584, L79
Maeder, A., Grebel, E. K., & Mermilliod, J.-C. 1999, A&A, 346, 459
Majid, W. A., Lamb, R. C., & Macomb, D. J. 2004, ApJ, 609, 133
McBride, V. A., Coe, M. J., Negueruela, I., Schurch, M. P. E., & McGowan, K. E. 2008, MNRAS, 388, 1198

McGowan, K. E., et al. 2008, MNRAS, 383, 330
Novara, G., La Palombara, N., Carangelo, N., et al. 2006, A&A, 448, 93
Rajoelimanana, A. F., Charles, P. A., & Udalski, A. 2011, MNRAS, 413, 1600
Russell, S. C., & Dopita, M. A. 1992, ApJ, 384, 508
Sasaki, M., Pietsch, W., & Haberl, F. 2003, A&A, 403, 901
Schmidtke, P. C., Cowley, A. P., Levenson, L., & Sweet, K. 2004, AJ, 127, 3388
Shtykovskiy, P., & Gilfanov, M. 2005, MNRAS, 362, 879
Shtykovskiy, P. E., & Gilfanov, M. R. 2007, Astronomy Letters, 33, 437
Sidoli, L. 2010, American Institute of Physics Conference Series, 1314, 271
Stanimirovic, S., Staveley-Smith, L., Dickey, J. M., Sault, R. J., & Snowden, S. L. 1999, MNRAS, 302, 417
Strüder, L., Briel, U., Dennerl, K., et al. 2001, A&A, 365, L18
Turner, M. J. L., Abbey, A., Arnaud, M., et al. 2001, A&A, 365, L27
Ubertini, P., et al. 2003, A&A, 411, L131
Wilms, J., Allen, A., & McCray, R. 2000, ApJ, 542, 914
Winkler, C., et al. 2003, A&A, 411, L1
Zaritsky, D., Harris, J., Thompson, I. B., Grebel, E. K., & Massey, P. 2002, AJ, 123, 855